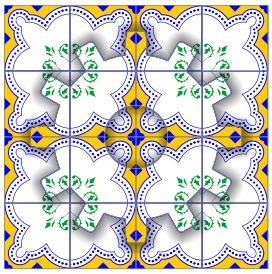

ABCM
Associação Brasileira de Engenharia e Ciências Mecânicas
CONEM 2012 «Engenharia em destaque»
VII Congresso Nacional de Engenharia Mecânica
São Luís - Maranhão - Brasil
31 de julho a 03 de agosto
www.abcm.org.br/conem2012

COMPRESSIBILITY EFFECTS ON THE FLOWFIELD STRUCTURE OF RAREFIED HYPERSONIC FLOW OVER FORWARD-FACING STEPS

Paulo H. M. Leite, phmineiro@lcp.inpe.br[1]
Wilson F. N. Santos, wilson@lcp.inpe.br[1]

[1]Combustion and Propulsion Laboratory, National Institute for Space Research (INPE), Cachoeira Paulista-SP, 12630-000 BRAZIL

Abstract. *Hypersonic flow over forward-facing steps is examined for a range of freestream Mach number from 5 to 25 at zero-degree angle of incidence. The work is motivated by interest in assessing the impact of surface discontinuities on hypersonic configurations in the Earth reentry. The Direct Simulation Monte Carlo (DSMC) method has been employed in order to examine the flowfield structure on these forward-facing steps. The results presented highlight some significant differences on the primary properties due to variations on the step frontal-face height and on the freestream Mach number. Interesting features observed on the velocity, density, pressure, and temperature profiles showed that small frontal-face thickness, compared to the freestream mean free path, still has important effects on the flowfield structure for the freestream Mach number range investigated.*

Keywords: *DSMC, Hypersonic Flow, Rarefield Flow, Forward-Facing Step.*

1. INTRODUCTION

The presence of surface discontinuities in modern aerodynamics configurations occurs as a desired or undesired design feature. Hypersonic flow over surface discontinuities, such as protuberances (Bertram and Wiggs, 1963; Bertram *et al.*, 1967; Mazaheri and Wood, 2009), notches (Charwat, 1971; Howell and Korst, 1971), cavities (Charwat *et al.*, 1961a,b; Everhart, 2009; Morgenstern Jr. and Chokani, 1994; Pan and Acrivos, 1967), gaps (Bertin and Goodrich, 1980; Hinderks *et al.*, 2004; Hinderks and Radespiel, 2006; Petley *et al.*, 1984; Vharbonnier and Boerrigter, 1993) or steps may cause locally thermal and aerodynamic loads that may dramatically exceed those in a smooth contour. In order to operate safely, these loads have to be predicted correctly. This can be done either by experiments that are often very expensive for real flight conditions or by numerical simulation, which is getting continuously increasing importance.

For the particular case of steps, there is nowadays a rather extensive literature dealing with forward-facing step flows. In general, these research studies have been conducted in order to understand, among others, the physical aspects of a laminar or turbulent boundary layer in a subsonic (Camussi *et al.*, 2008; Chapman *et al.*, 1958; Stüer et al., 1999), supersonic (Bogdonoff and Kepler, 1955; Chapman *et al.*, 1958; Driftmyer, 1973; Rogers and Berry, 1965; Uebelhack, 1969; Zukoski, 1967) or hypersonic (Grotowsky and Ballmann, 2000; Nestler *et al.*, 1969; Pullin and Harvey, 1977; Wilkinson and East, 1968) flow past to this type of discontinuity, characterized by a sudden change on the surface slope.

Nevertheless, the major interest in these research studies on forward-facing step has gone into considering laminar or turbulent flow in the continuum flow regime. However, there is little understanding of the physical aspects of rarefied hypersonic flows past to steps related to the severe aerothermodynamic environment associated to a reentry vehicle. In this scenario, Leite and Santos (Leite and Santos, 2009a,b) have investigated forward-facing steps situated in a rarefied hypersonic flow by employing the Direct Simulation Monte Carlo (DSMC) method. The studies were motivated by the interest in investigating the frontal-face height effect on the flowfield structure and on the aerodynamic surface properties in the transition flow regime, i.e., between the continuum flow and the free collision flow regime. The analysis showed that the hypersonic flow past a forward-facing step was characterized by a strong compression ahead of the frontal face. The analysis also showed that disturbances upstream the step depended on changes in the frontal-face height of the steps. In addition, results showed that the separation point and the pre-separation region relied on the frontal-face height.

The present investigation was undertaken in an attempt to extend further the previous analysis (Leite and Santos, 2009a,b) by investigating the impact of the freestream Mach number on the flowfield structure for a family of forward-facing step. In this scenario, the primary goal of this paper is to assess the sensitivity of the primary properties, such as

velocity, density, pressure and temperature, due to changes on the freestream Mach number and on the frontal-face height. A detailed and careful effort is made to provide a comprehensive description of the flow with special relevance to the particular case where the step height is less than the boundary-layer thickness. Physically, some of the molecules that collide with the frontal face of the steps are reemitted in the upstream direction. These reflected molecules collide with the incoming freestream molecules, thereby altering the flow about the forward-facing step. In addition, the importance of this effect is in part conditioned by the frontal-face thickness as well as by the velocity of the incoming freestream molecules. The focus of the present study is the low-density region in the upper atmosphere, where numerical gaskinetic procedures are available to simulate hypersonic flows. Therefore, the DSMC method will be employed to calculate the hypersonic two-dimensional flow on the steps.

1.1 GEOMETRY DEFINITION

In the present account, surface discontinuities present on reentry hypersonic configurations are modeled by a forward-facing step as defined in the previous studies (Leite and Santos, 2009a,b). By considering that the step frontal-face h is much smaller than the nose radius R of a reentry vehicle, i.e., $h/R \ll 1$, then the hypersonic flow over the step may be considered as a hypersonic flow over a flat plate with a forward-facing step. Figure 1(a) displays a schematic view of the model employed and presents the important geometric parameters.

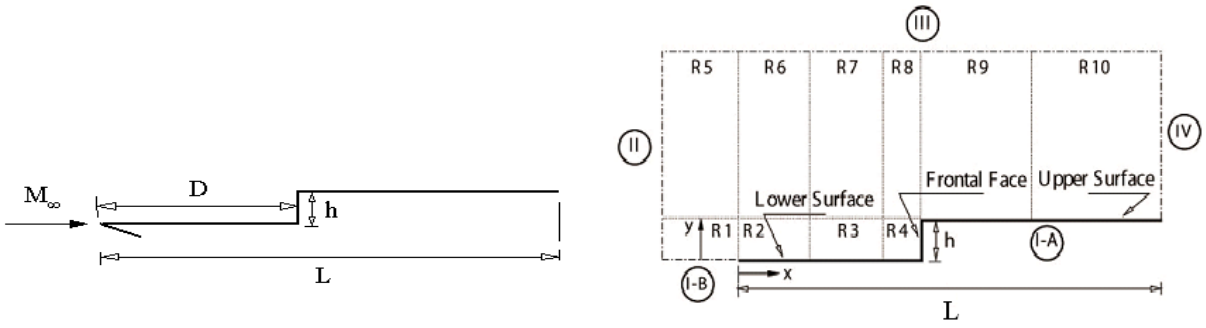

(a) Forward-facing step

(b) Computational domain

Figure 1: Drawing illustrating (a) a schematic view of the forward-facing step and (b) the computational domain.

According to Fig. 1(a), M_∞ represents the freestream Mach number, h is the frontal-face height, L refers to the total length of the forward-facing step, and D stands for the location of the step. It was considered that the forward-facing step is infinitely long but only the length L is considered. It was assumed a frontal-face height h of 3, 6, and 9 mm, which correspond to $H = h/\lambda_\infty$ of 3.23, 6.46, and 9.69, D/λ_∞ of 50 and L/λ_∞ of 100, where λ_∞ is the freestream mean free path.

2. COMPUTATIONAL METHOD AND PROCEDURE

It is well known that the DSMC method introduced by Bird (1994) has become a reliable and efficient kinetic approach for modeling rarefied gas flows. Typical applications include microelectromechanical systems (MEMS) devices, low-pressure plasma material-processing reactors, spacecraft propulsion and contamination, high altitude rockets plumes, and reentry vehicles. Although these applications encompass a wide range of spatial and temporal scales, they are connected by the same underlying physics of moderate or high Knudsen number flows. The Knudsen number Kn is de ratio of the gas mean free path λ to a characteristic length scale of the problem. It is generally accepted that the rarefied transition flow regime lies in the range of $0.01 < Kn < 10$. The transition flow regime is the category of flow that falls between the continuum regime, where the Navier-Stokes equations are valid, and the free molecular regime, which is the limit of infinite Knudsen number.

The DSMC method is a computer simulation technique to solve the Boltzmann equation by modeling a real gas flow by using a representative set of molecules. The method employs thousands or millions of simulated molecules in order to reproduce the behavior of a far larger number of real molecules within the flow. The strategy of the method is to use a computer to track the trajectory of these simulated particles, where each simulated particle represents a fixed number of real gas particles. The direct simulation of the physical processes is in contrast with computation fluid dynamics (CFD) method, that is applied to the mathematical equations that model the physical processes, but is similar to the molecular-dynamics method in that a large number of simulated molecules are followed simultaneously. The essential difference is

that the intermolecular collisions are dealt with on a probabilistic rather than a deterministic basis.

Collisions in the present DSMC code are simulated with the variable hard sphere (VHS) molecular model (Bird, 1981),and the no time counter (NTC) collision sampling technique (Bird, 1989). Repartition energy among translational and internal modes is controlled by the Borgnakke-Larsen statistical model (Borgnakke and Larsen, 1975). For the present work, the simulations are performed using a non-reacting gas model for a constant freestream gas composition consisting of 76.3% of N_2 and 23.7% of O_2, while considering energy exchange between translational, rotational and vibrational modes.

3. FREESTREAM AND FLOW CONDITIONS

The flow conditions represent those experienced by a reentry vehicle at an altitude of 70 km. This altitude is associated with the transitional flow regime, which is characterized by the overall Knudsen number of the order of or larger than 10^{-2}. In this manner, the freestream conditions employed in the present calculations are those defined in the previous studies (Leite and Santos, 2009a,b) and listed in Tab. 1, and the gas properties (Bird, 1994) considered in the simulation are shown in Tab. 2.

Table 1: Freestream flow conditions

Altitude (km)	T_∞(K)	p_∞(N/m^2)	ρ_∞(kg/m^3)	μ_∞(Ns/m^2)	n_∞(m^{-3})	λ_∞(m)
70	219.69	5.582	8.753×10^{-5}	1.455×10^{-5}	1.8192×10^{21}	9.285×10^{-4}

The freestream velocity U_∞ is assumed to be constant at 1485.3 m/s, 4527.8 m/s, and 7546.5 m/s, which corresponds to a freestream Mach number M_∞ of 5, 15 and 25, respectively. The wall temperature T_w is assumed constant at 880 K. This temperature is chosen to be representative of the surface temperature near the stagnation point of a reentry vehicle and is assumed to be uniform over the forward-facing step surface.

Table 2: Gas properties

	X	m (kg)	d (m)	ω
O_2	0.237	5.312×10^{-26}	4.01×10^{-10}	0.77
N_2	0.763	4.650×10^{-26}	4.11×10^{-10}	0.74

It is important to mention that the surface temperature is low compared to the stagnation temperature of the air. This assumption seems reasonable since practical surface material will probably be destroyed if surface temperature is allowed to approach the stagnation temperature.

By assuming the frontal-face height h as the characteristic length, the Knudsen number Kn_h corresponds to 0.3095, 0.1548 and 0.1032 for height h of 3, 6 and 9 mm, respectively. Finally, the Reynolds number Re_h, also based on the frontal-face height h and on conditions in the undisturbed stream, cover from 27 to 409 for the cases investigated.

4. COMPUTATIONAL DOMAIN AND GRID

In order to implement the particle-particle collisions, the flowfield around the forward-facing step is divided into an arbitrary number of regions, which are subdivided into computational cells. The cells are further subdivided into subcells, two subcells/cell in each coordinate direction. The cell provides a convenient reference for the sampling of the macroscopic gas properties, while the collision partners are selected from the same subcell for the establishment of the collision rate. Therefore, the physical space network is used to facilitate the choice of molecules for collisions and for the sampling of the macroscopic flow properties such as density, velocity, pressure, temperature, etc.

A schematic view of the computational domain is depicted in Fig. 1(b). According to this figure, side I-A is defined by the forward-facing step surface. Diffuse reflection with complete thermal accommodation is the condition applied to this side. In a diffuse reflection, the molecules are reflected equally in all directions, and the final velocity of the molecules is randomly assigned according to a half-range Maxwellian distribution determined by the wall temperature. Side I-B represents a plane of symmetry, where all flow gradients normal to the plane are zero. At the molecular level, this plane is equivalent to a specular reflecting boundary. Sides II and III are the freestream side through which simulated molecules enter and exit. Depending on the case investigated, side II is positioned from $5\lambda_\infty$ to $10\lambda_\infty$ upstream of the flat-plate leading edge, and side III defined from $30\lambda_\infty$ to $52\lambda_\infty$ above the step upper surface. Finally, the flow at the downstream outflow boundary, side IV, is predominantly supersonic and vacuum condition is specified (Bird, 1994). At this boundary, simulated molecules can only exit.

DSMC results depend on the cell size chosen, on the time step as well as on the number of particles per computational cell. In the DSMC code, the linear dimensions of the cells should be small in comparison with the length scale of the macroscopic flow gradients normal to the streamwise directions, which means that the cell dimensions should be the order of or smaller than the local mean free path (Alexander $et\ al.$, 1998, 2000). The time step should be chosen to

Table 3: Region Dimensions ($x \times y$) and number of cells [$x \times y$] for cases H of 3.23, 6.46, and 9.69 and freestream Mach number of 25.

	H = 3.23	**H = 6.46**	**H = 9.69**
R1	$(5\lambda_\infty \times 3.23\lambda_\infty)[10 \times 10]$	$(5\lambda_\infty \times 6.46\lambda_\infty)[10 \times 20]$	$(5\lambda_\infty \times 9.69\lambda_\infty)[10 \times 30]$
R2	$(20\lambda_\infty \times 3.23\lambda_\infty)[40 \times 30]$	$(20\lambda_\infty \times 6.46\lambda_\infty)[40 \times 50]$	$(20\lambda_\infty \times 9.69\lambda_\infty][40 \times 60]$
R3	$(20\lambda_\infty \times 3.23\lambda_\infty)[40 \times 30]$	$(20\lambda_\infty \times 6.46\lambda_\infty)[40 \times 50]$	$(20\lambda_\infty \times 9.69\lambda_\infty)[60 \times 60]$
R4	$(10\lambda_\infty \times 3.23\lambda_\infty)[60 \times 70]$	$(10\lambda_\infty \times 6.46\lambda_\infty)[110 \times 120]$	$(10\lambda_\infty \times 9.69\lambda_\infty)[120 \times 140]$
R5	$(5\lambda_\infty \times 30\lambda_\infty)[10 \times 40]$	$(5\lambda_\infty \times 34\lambda_\infty)[10 \times 50]$	$(5\lambda_\infty \times 42\lambda_\infty)[10 \times 60]$
R6	$(20\lambda_\infty \times 30\lambda_\infty)[30 \times 40]$	$(20\lambda_\infty \times 34\lambda_\infty)[30 \times 50]$	$(20\lambda_\infty \times 42\lambda_\infty)[30 \times 60]$
R7	$(20\lambda_\infty \times 30\lambda_\infty)[30 \times 40]$	$(20\lambda_\infty \times 34\lambda_\infty)[30 \times 50]$	$(20\lambda_\infty \times 42\lambda_\infty)[30 \times 60]$
R8	$(10\lambda_\infty \times 30\lambda_\infty)[30 \times 50]$	$(10\lambda_\infty \times 34\lambda_\infty)[30 \times 60]$	$(10\lambda_\infty \times 42\lambda_\infty)[30 \times 80]$
R9	$(25\lambda_\infty \times 30\lambda_\infty)[60 \times 70]$	$(25\lambda_\infty \times 34\lambda_\infty)[70 \times 90]$	$(25\lambda_\infty \times 42\lambda_\infty)[70 \times 90]$
R10	$(25\lambda_\infty \times 30\lambda_\infty)[60 \times 80]$	$(25\lambda_\infty \times 34\lambda_\infty)[60 \times 80]$	$(25\lambda_\infty \times 42\lambda_\infty)[70 \times 80]$

be sufficiently small in comparison with the local mean collision time (Garcia and Wagner, 2000; Hadjiconstantinou, 2000). Finally, the number of simulated particles has to be large enough to make statistical correlations between particles insignificant.

As part of the verification process, a grid independence study was made with three different structured meshes, coarse, standard and fine, in each coordinate direction. The effect of altering the cell size in the x- and y-directions was investigated for a coarse and fine grids with, respectively, 50% less and 100% more cells with respect to the standard grid. Table 3 summarizes the main characteristics for the standard grid related to ten regions, from R1 to R10 in Fig. 1(b), for the frontal-face height H of 3.23, 6.46, and 9.69, and for the M_∞ = 25 case. In this way, for H of 3.23, 6.46, and 9.69, the total number of cells correspond, respectively, to 20,000, 33,800, and 41,600 cells.

A discussion of the verification process, effects of cell size, time step and number of molecules on the aerodynamic surface quantities for the forward-facing steps presented herein, is described in detail in Leite (2009). Furthermore, as part of the validation process, results for density, velocity and translational temperature were compared with those obtained from other established DSMC code and experimental data in order to ascertain how well the DSMC code employed in this study is able to predict hypersonic flow in a flat plate. Details of this comparison is also presented in Leite (2009).

5. COMPUTATIONAL RESULTS AD DISCUSSION

5.1 Velocity Field

Distribution of tangential velocity profiles for three sections along the lower surface and their dependence on the step frontal-face thickness are illustrated in Figs. 2 and 3 for freestream Mach number of 5 and 25, respectively. In this set of plots, the velocity ratio corresponds to the velocity u normalized by the freestream velocity U_∞, X and Y correspond, respectively, to the length x and height y normalized by the freestream mean free path λ_∞. It is important to mention that U_∞ is different for each freestream Mach number case and, therefore, the comparison is made in terms of ratio. As a basis of comparison, the tangential velocity profiles for the flat-plate case are illustrated in the plots corresponding to M_∞ = 25 case. It is also important to remark that the steps are located at section X = 50. In addition, it is noteworthy that results of the velocity profiles for M_∞ = 15 case are intermediate to the other Mach number cases, and therefore, they will no be shown.

According to this set of plots, it is clearly seen that the frontal-face thickness as well as the freestream Mach number influences the flowfield far upstream. This domain of influence increases with increasing the step frontal-face thickness and with decreasing the freestream Mach number. The frontal-face thickness effect results from the upstream diffusion of particles that are reflected from the step frontal face. Consequently, by increasing the step frontal-face height leads to significantly larger disturbance upstream of the step. On the other hand, with decreasing the freestream Mach number, particles reflecting from the step frontal face diffuse further upstream due to the lower density at the vicinity of the step frontal face, as will be seen subsequently. This features are notable in Figs. 2(a) and 3(a). This is explained by the fact that a density decrease corresponds to a mean free path increase. As a result, the molecules travel a larger distance between collisions, and the effect due to the presence of the step is felt more upstream.

Also of great significance is the flow peculiarity observed in the plots for sections $X \geq 38$. For these sections, the velocity profiles indicate negative velocities near the lower surface, characterizing a recirculation region at the vicinity of the frontal face. For section $X = 38$, negative velocity occurs only for the H = 9.69 case, and for section $X = 48$, for the three frontal-face heights investigated, as displayed by the magnified view shown in Figs. 2 and 3.

In order to emphasize important features in the flowfield structure, streamline traces at the vicinity of the steps are demonstrated in Figs. 4 and 5 for freestream Mach number of 5 and 25, respectively. In this group of contour maps, Y_h

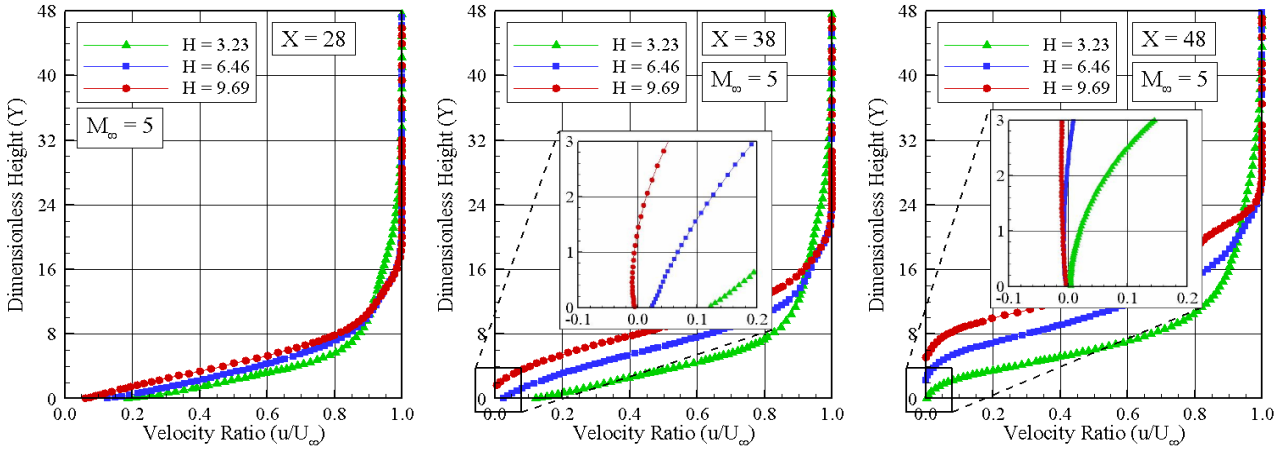

Figure 2: Distribution of tangential velocity (u/U_∞) along the lower surface of the forward-facing step for freestream Mach number of 5.

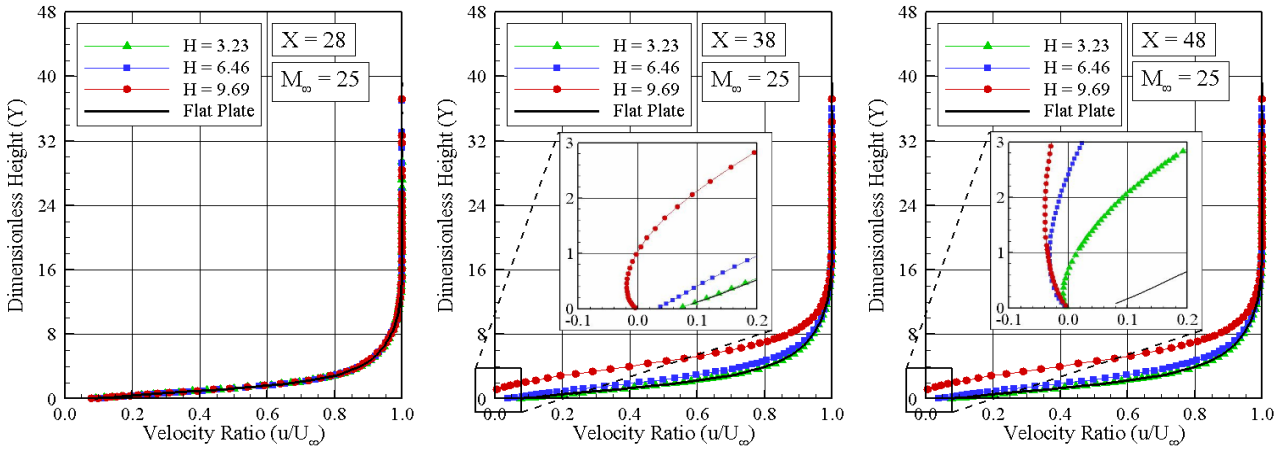

Figure 3: Distribution of tangential velocity (u/U_∞) along the lower surface of the forward-facing step for freestream Mach number of 25.

stands for the vertical distance y normalized by the step height h, and X'_h refers to the horizontal distance $(x - D)$ also normalized by the step height h. In this context, the reference frame was moved to the step position. According to this set of contour maps, it is clearly noticed the presence of a recirculation region at the vicinity of the frontal face of the steps, for the conditions investigated in the present account.

The following features are also notable in the plots demonstrated in Figs. 4 and 5. For the H = 3.23 case and Mach number of 25, streamlines are basically parallel to the lower surface at section X'_h = - 4.0. Therefore, it is thus firmly established that the flowfield at sections $X'_h \leq$ - 4.0 has no idea about the presence of the step. In contrast, for the H = 6.46 and 9.69 cases, streamlines are inclined upward at the same section, an indication that the flowfield knows about the presence of the steps positioned downstream along the lower surface. This information about the presence of the steps is communicated upstream by means of molecular collisions.

Another flow peculiarity is related to the recirculation region. It may be inferred by visual inspection that the recirculation region increases with increasing the step height h, or by increasing the Reynolds number Re_h, not only along the lower surface but also along the frontal face. This behavior differs from that one observed in a continuum flow regime. Based on an experimental investigation, Camussi *et al.* (2008) pointed out that the separation region occurs independently of the Reynolds number Re_h. They found that the separation region is of the order of h upstream the step and approximately a half h size along the frontal face.

Still referring to Figs. 4 and 5, it is quite apparent that, after the flow separation on the lower surface, the flow reattaches on the frontal face at the vicinity of the step shoulder. For the steps under investigation, the separation point x_s and the reattachment point y_r on the frontal face are obtained on the basis of zero skin friction coefficient, $C_f = 0$ (or τ_w = 0). Table 4 tabulates x_s and y_r as a function of the dimensionless height H and of the freestream Mach number. In this table,

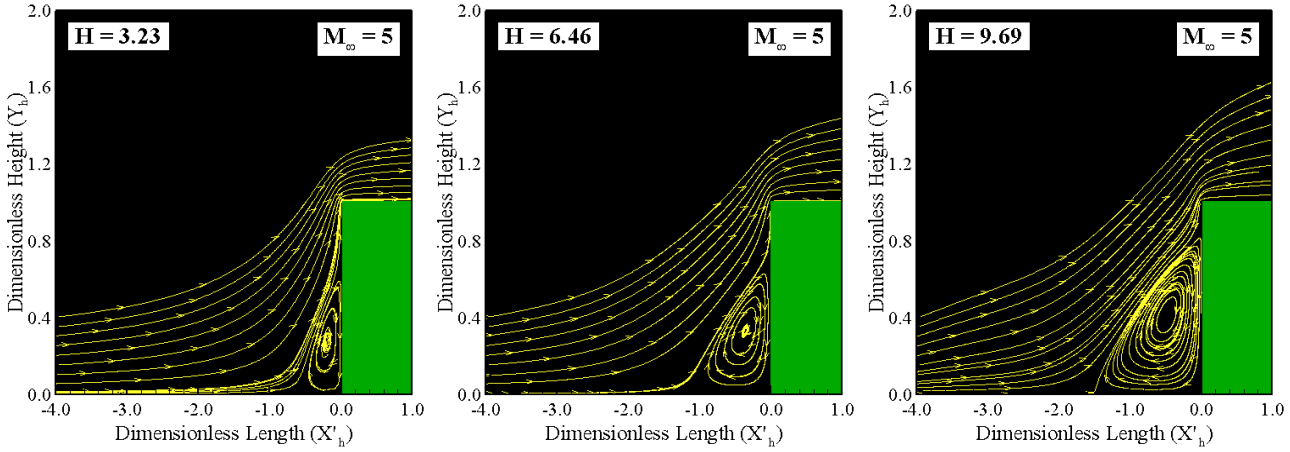

Figure 4: Distribution of streamline traces at the vicinity of the forward-facing step for dimensionless frontal-face height H of (a) 3.23, (b) 6.46, and (c) 9.693 for freestream Mach number of 5.

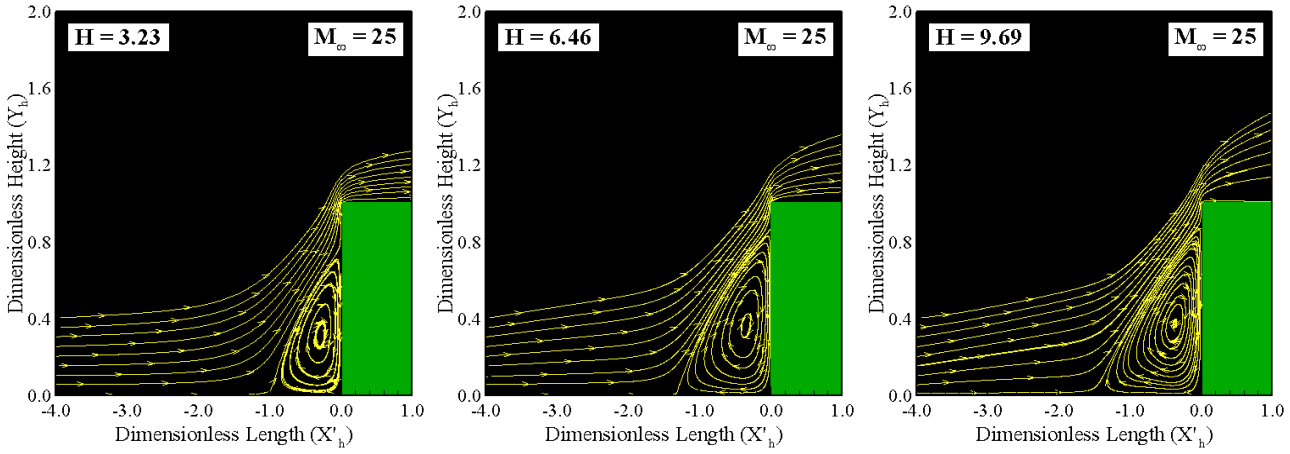

Figure 5: Distribution of streamline traces at the vicinity of the forward-facing step for dimensionless frontal-face height H of (a) 3.23, (b) 6.46, and (c) 9.693 for freestream Mach number of 25.

X_s and X_{sh} represent, respectively, the separation point x_s normalized by the freestream mean free path λ_∞ and by the step height h. Similarly, Y_r and Y_{rh} stand for the reattachment point y_r normalized by λ_∞ and h, respectively.

Table 4: Separation point (X_s;X_{sh}) and the reattachment point [y_r;Y_{rh}] as a function of the Mach number.

H	$M_\infty = 5$	$M_\infty = 15$	$M_\infty = 25$
3.23	(49.40;15.29) [2.80;0.86]	(48.79;13.59) [2.67;0.83]	(48.26;14.94) [2.69;0.83]
6.46	(44.52; 6.89) [4.85;0.75]	(42.76; 6.62) [5.70;0.88]	(42.76; 6.62) [5.66;0.88]
9.69	(36.82; 3.80) [8.03;0.83]	(36.73; 3.79) [8.88;0.92]	(37.20; 3.84) [8.72;0.89]

5.2 Density Field

The distribution of density profiles along the lower surface of the step is displayed in Figs. 6 and 7 for freestream Mach number of 5 and 25, respectively, and parameterized by the dimensionless step height H. Similar to tangential velocity profiles, density profiles are shown in this group of plots for three sections defined by X = 28, 38 and 48. In this group of plots, density ratio refers to density ρ normalized by the freestream density ρ_∞. Again, X represents the distance x normalized by the freestream mean free path λ_∞, and Y the distance y above the lower surface also normalized by λ_∞.

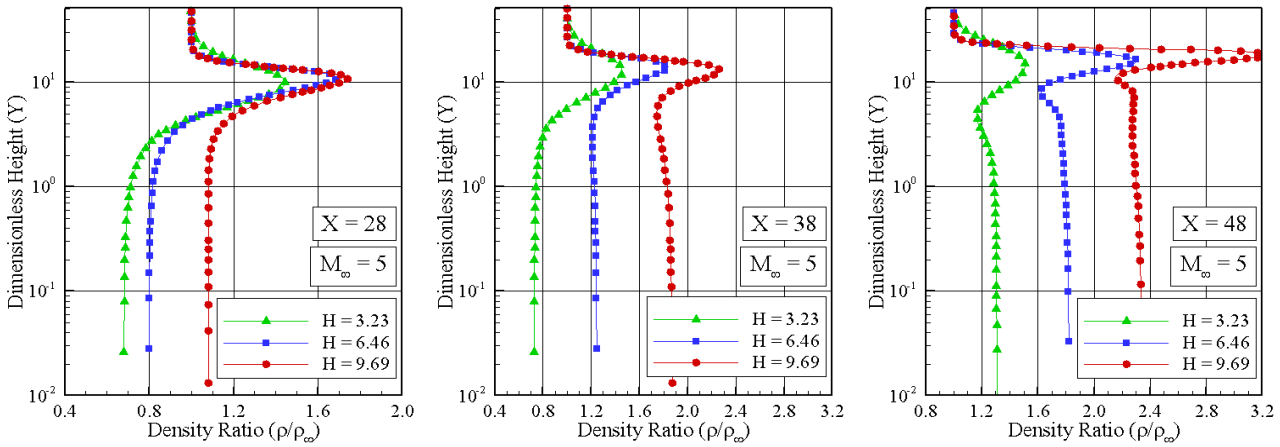

Figure 6: Distribution of density ratio (ρ/ρ_∞) profile along the lower surface of the forward-facing step for freestream Mach number of 5.

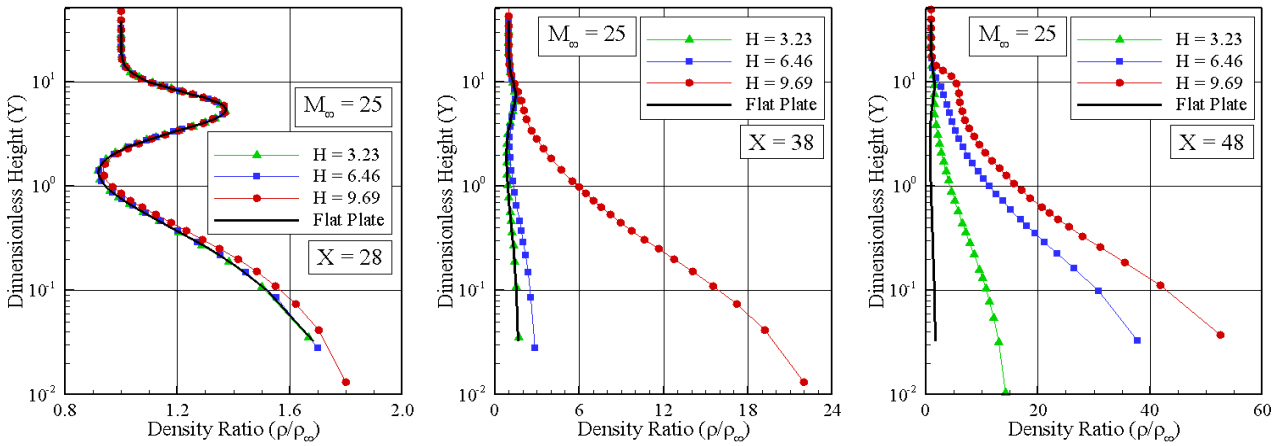

Figure 7: Distribution of density ratio (ρ/ρ_∞) profile along the lower surface of the forward-facing step for freestream Mach number of 25.

As a basis of comparison, density ratio profiles for the flat-plate case are also presented in the same group of plots for M_∞ = 25 case. Due to the large range of variation for the ratio ρ/ρ_∞ along the lower surface of the step, the scale in the x-direction may differ from one plot to another.

Looking first to Fig. 6, which corresponds to freestream Mach number of 5, it is observed that the upstream disturbance caused by the steps is felt by the density profile in the three sections. As expected, the disturbance caused by the steps is felt more upstream with increasing the step frontal-face thickness. Also, it may be recognized from this set of plots that density increases slightly as compared to the freestream density as the flow approaches the steps. As a base of comparison, at section X = 48, the density ratio ρ/ρ_∞ is around 1.3, 1.8 and 2.3 for H of 3.23, 6.46, and 9.69, respectively.

Turning next to Fig. 7, for freestream Mach number of 25, it is seen that the upstream disturbance caused by the step with H = 9.69 is felt by the density profile at section X = 38. In contrast, there is no indication that the density profile be affected by the presence of the step with H = 3.23. It should be mentioned in this context that, for $X < 28$, the density profiles for the step cases are identical to those for the flat-plate case, i.e., a flat plate without a step. In addition, it is also noted that density dramatically increases as the flow approaches the step, i.e., the density ρ increased by an order of magnitude, almost two, when compared to the freestream density ρ_∞. For comparison purpose, the density ratio ρ/ρ_∞ is around 32.9, 56.2 and 72.3 for H of 3.23, 6.46, and 9.69, respectively, at the step base. This density increase is in contrast with that for M_∞ = 5 case. It should be mentioned in this context that this density rise at the vicinity of the frontal face is a characteristic observed in blunt-body reentry flow, known as a cold-wall flow. Usually, in a reentry flow, the wall temperature T_w is low compared to the stagnation temperature T_o. For this particular investigation, this ratio is 0.032 for M_∞ = 25 case.

Still referring to Fig. 7, it is quite apparent that the density ratio experiences significant changes in the direction

perpendicular to the lower surface of the step. For section $X = 28$, the density ratio is high adjacent to the wall, $Y \approx 0$, and rapidly decreases inside a layer of thickness around one to two freestream mean free paths, where the density ratio is less than one. It means that the density ρ is smaller than the freestream density ρ_∞. After that, as Y increases, the density ratio increases significantly at a maximum value, $\rho/\rho_\infty \approx 1.4$, inside the shock wave. Afterwards, density decreases again and reaches the freestream density value as $Y \to \infty$. This behavior, high density ratio at the wall and inside the shock wave, and low density ratio between them, is usually observed when the temperature of the body surface is much lower than the stagnation temperature of the freestream gas. Consequently, the gas near the wall tends to be very cold and denser than the rest of the gas in the boundary layer. Furthermore, as will be seen subsequently, the maximum kinetic temperature inside the shock wave takes place in a section corresponding to $1 < Y < 2$. Consequently, the density decreases in this region, as shown in Fig. 7(a).

5.3 Pressure Field

The distribution of pressure p for three sections along the lower surface of the step is illustrated in Figs. 8 and 9 for freestream Mach number of 5 and 25, respectively, as a function of the dimensionless step height H. In this set of plots, the pressure ratio corresponds to the pressure p normalized by the freestream pressure p_∞. X and Y are dimensionless variables as defined previously in the density profiles. Moreover, for comparative purpose, pressure profiles for the flat-plate case are also exhibited in the plots for M_∞ = 25 case. It is important to emphasize that, due to the large range of variation for the ratio p/p_∞ along the lower surface of the step, the scale in the x-direction may differ from one plot to another.

Based on Figs. 8 and 9, it is noticed that pressure profiles follow a similar behavior as compared to that presented by density profiles in the sense that pressure profiles present a slightly increase in the pressure ratio along the lower surface for M_∞ = 5 case, and a significant pressure ratio increase for the M_∞ = 25 case. In addition, the impact of the step frontal-face thickness on the upstream disturbance related to pressure profiles is similar to that for density profiles in the sense that the pressure profiles are not affected at section $X = 28$ for M_∞ = 25 case, and they are affected for M_∞ = 5 case for the frontal-face thickness investigated.

Particular attention is paid to the pressure profiles for freestream Mach number of 25. For this high Mach number, the pressure profiles for the three steps are basically identical to those for the flat-plate case at section $X = 28$, indicating that the pressure field has not been affected yet by the presence of the steps. For the section $X = 38$, the pressure field is already affected by the presence of the steps with height H of 6.46 and 9.69. In contrast, no effect is observed in the pressure profile at section $X = 38$ due to the presence of the step with height H of 3.23. On the other hand, at section $X = 48$, pressure profiles for the step cases differ considerable from that for the flat-plate case. As expected, the upstream disturbance increases with the step frontal-face rise. It is also noticed that the pressure ratio dramatically increases as the flow approaches the step base. It is seen that the pressure p increased two orders of magnitude as compared to the freestream pressure p_∞. For illustration purpose, at the step base, the pressure ratio p/p_∞ is 142, 230, and 293 for height H of 3.23, 4.46, and 9.69, respectively. Consequently, it may be inferred in passing that particular attention should be paid to the step base in terms of pressure loads, since the vicinity of the step base represents a zone of strong compression for flow with high freestream Mach number.

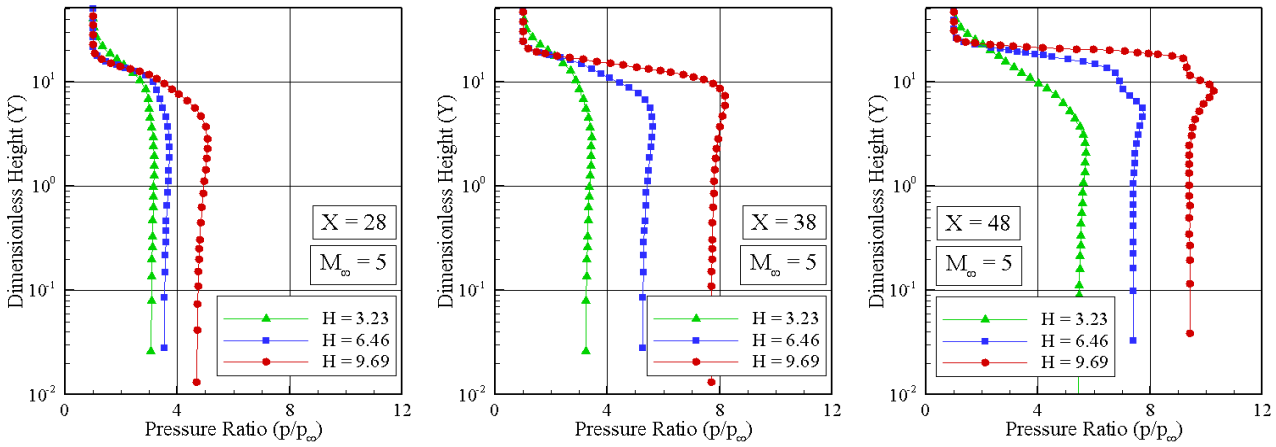

Figure 8: Distribution of pressure ratio (p/p_∞) profile along the lower surface of the forward-facing step for freestream Mach number of 5.

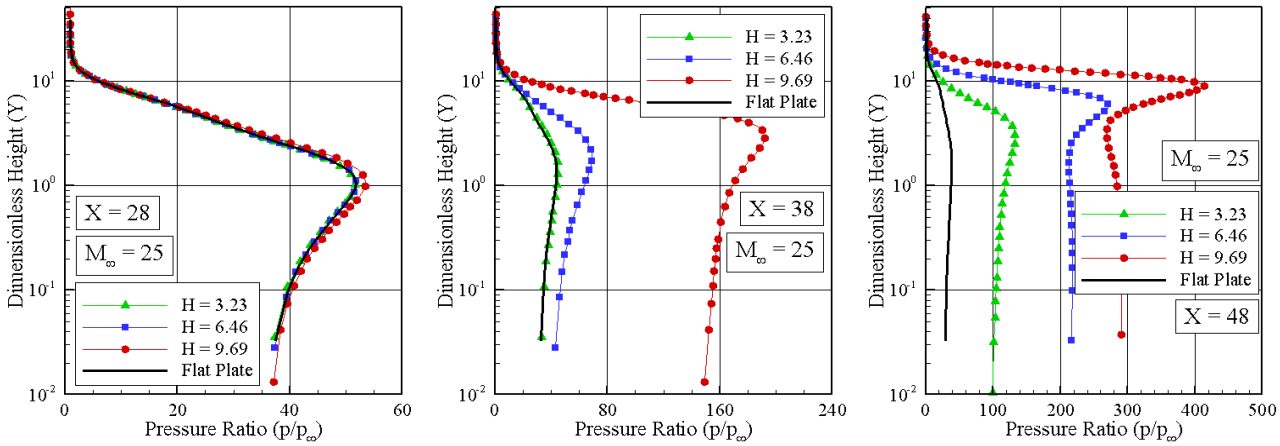

Figure 9: Distribution of pressure ratio (p/p_∞) profile along the lower surface of the forward-facing step for freestream Mach number of 25.

5.4 Temperature Field

Kinetic temperature profiles along the lower surface for sections X of 28, 38 and 48 are displayed in Figs. 10 and 11 for freestream Mach number of 5 and 25, respectively. In this set of diagrams, temperature ratio stands for the translational temperature T_T, rotational temperature T_R, vibrational temperature T_V or overall temperature T_O normalized by the freestream temperature T_∞. Also, filled and empty symbols refer to temperature distributions for frontal-face height H of 3.23 and 9.69, respectively. Temperature profiles for the H = 6.46 case are intermediate to these two cases, and they will not be shown. In addition, for M_∞ = 25 case, the solid lines correspond to the kinetic temperature profiles for the flat-plate case.

On examining Figs. 10 and 11, it is quit apparent that thermodynamic non-equilibrium occurs throughout the shock layer, as shown by the lack of equilibrium of the translational and internal kinetic temperatures. Thermal non-equilibrium occurs when the temperatures associated with translational, rotational, and vibrational modes of a polyatomic gas are different one to each other. The overall kinetic temperature T_O is equivalent to the thermodynamic temperature only in thermal equilibrium conditions. In such a context, it should be noticed that the ideal gas equation of state does not apply to this temperature in a non-equilibrium situation.

In a thermodynamic non-equilibrium gas, the overall kinetic temperature T_O is defined as the weighted mean of the translational and internal temperatures (Bird, 1994) as being,

$$T_O = \frac{\zeta_T T_T + \zeta_R T_R + \zeta_V T_V}{\zeta_T + \zeta_R + \zeta_V} \tag{1}$$

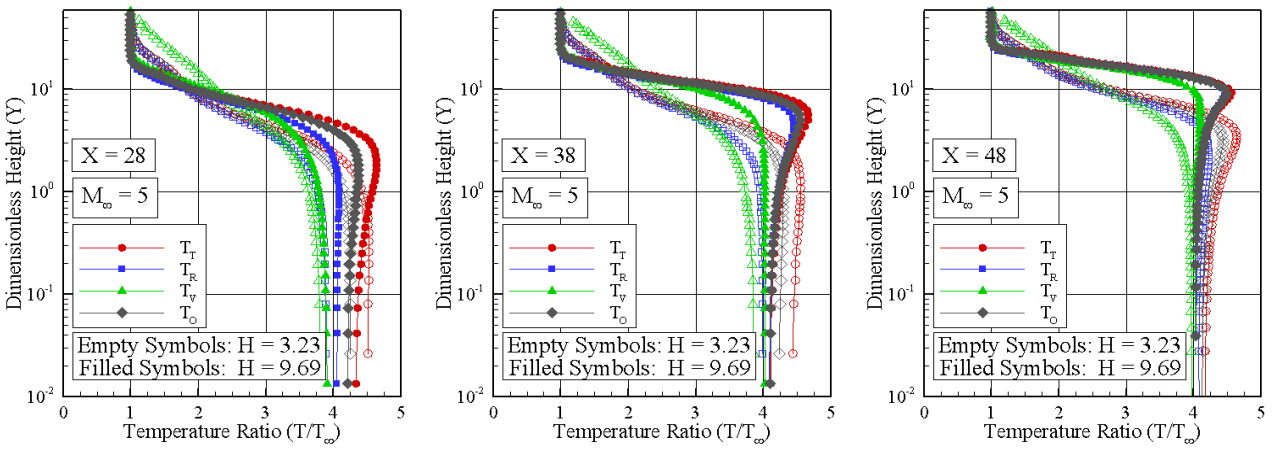

Figure 10: Distribution of kinetic temperature ratio (T/T_∞) profile along the lower surface of the forward-facing step for freestream Mach number of 5.

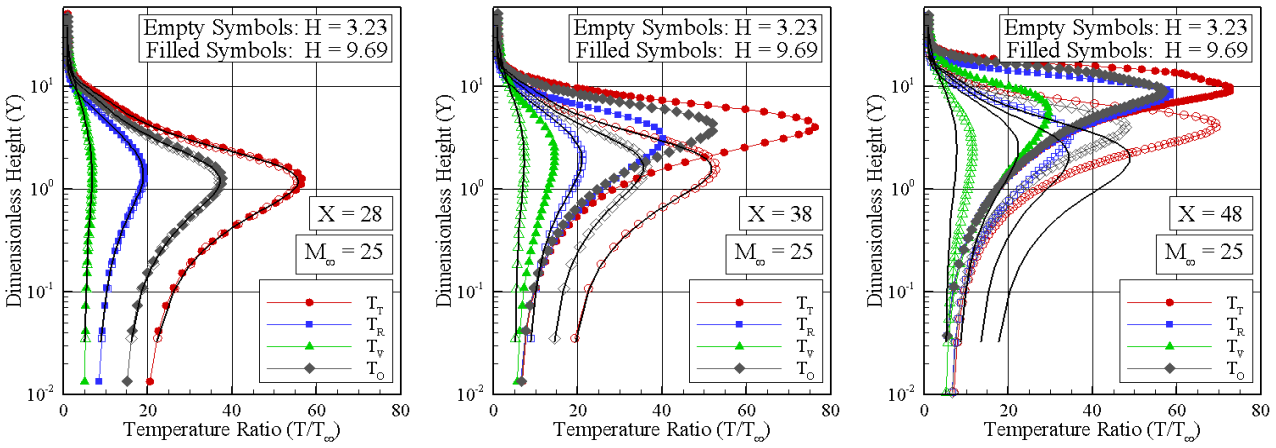

Figure 11: Distribution of kinetic temperature ratio (T/T_∞) profile along the lower surface of the forward-facing step for freestream Mach number of 25.

were ζ is the degree of freedom and subscript T, R and V stand for translation, rotation and vibration, respectively.

Still referring to Figs. 10 and 11, it is noticed that, in the undisturbed freestream far from the lower surface, $Y \to \infty$, the translational and internal kinetic temperatures have the same value and are equal to the thermodynamic temperature. Approaching the lower surface, say $2 < Y < 10$, the translational kinetic temperature rises to well above the rotational and vibrational temperatures and reaches a maximum value that relies on the section X and on the freestream Mach number. Since a large number of collisions is needed to excite molecules vibrationally from the ground state to the upper state, the vibrational temperature is seen to increase much more slowly than rotational temperature. Still further toward the lower surface, $Y \approx 0$, the translational, rotational, vibrational, and overall kinetic temperatures decrease, and reach values that depend on the section X as well as on the freestream Mach number. For section X = 28, the kinetic temperatures reach values on the wall that are above the wall temperature T_w ($\approx 4T_\infty$), resulting in a temperature jump as defined in continuum formulation. For section X = 38, the difference between translational temperature and internal temperatures for the H = 9.69 case indicates that the thermodynamic equilibrium is achieved close to the lower surface. Finally, for section X = 48, the kinetic temperatures basically reach the wall temperature T_w, and the thermodynamic equilibrium is achieved for the cases defined by H of 3.23 and 9.69.

6. CONCLUDING REMARKS

Computations of a rarefied hypersonic flow over forward-facing steps have been performed by using the Direct Simulation Monte Carlo (DSMC) method. The simulations provided information concerning the nature of the flowfield properties due to changes on the freestream Mach number and on the frontal-face height for a representative range of parameters. The freestream Mach number ranged from 5 to 25, and the frontal-face height ranged from 3 to 9 mm, which corresponded to Knudsen numbers in the transition flow regime.

It was found that the interaction point location and the separation region extent upstream the steps are a function of the frontal-face height and of the freestream Mach number. The analysis showed that the upstream disturbance due to the presence of the steps increased with increasing the frontal-face height and decreased with the freestream Mach number rise.

7. ACKNOWLEDGEMENTS

The authors would like to thank the financial support provided by CNPq (Conselho Nacional de Desenvolvimento Científico e Tecnológico) under Grant No. 473267/2008-0.

REFERENCES

Alexander, F. J., Garcia, A. L., and Alder, B. J., 1998. "Cell size dependence of transport coefficient in stochastic particle algorithms". *Physics of Fluids*, Vol. 10, pp. 1540–1542.

Alexander, F. J., Garcia, A. L., and Alder, B. J., 2000. "Erratum: Cell size dependence of transport coefficient in stochastic particle algorithms". *Physics of Fluids*, Vol. 12, pp. 731–731.

Bertram, M. H., and Wiggs, M. M., 1963. "Effect of surface distortions on the heat transfer to a wing at hypersonic speeds". *AIAA Journal*, Vol. 1, pp. 1313–1319.

Bertram, M. H., Weinstein, L. M., Cary Jr., A. M., and Arrington, J. P., 1967. "Heat transfer to wavy wall in hypersonic flow". *AIAA Journal*, Vol. 5, pp. 1760–1767.

Bertin, J. J., and Goodrich, W. D., 1980. "Aerodynamic heating for gaps in laminar and trasitional boundary layers". In *18th AIAA Aerospace Sciences Meeting and Exhibit*, AIAA Paper 80–0287, Pasadena, CA, USA, January 14–16,.

Bird, G. A., 1981. "Monte Carlo simulation in an engineering context". In Fisher, S. S., ed., *Progress in Astronautics and Aeronautics: Rarefied gas Dynamics*, Vol. 74, part I, AIAA New York, pp. 239–255.

Bird, G. A., 1989. "Perception of Numerical Method in Rarefied Gasdynamics". In Muntz, E. P., Weaver, D. P., and Capbell, D. H., eds., *Rarefied Gas Dynamics: Theoretical and Computational Techniques*, Vol. 118, Progress in Astronautics and Aeronautics, AIAA, New York, pp. 374–395.

Bird, G. A., 1994. *Molecular gas dynamics and the direct simulation of gas flows*, Oxford University Press.

Bogdonoff, S. M. and Kepler, C. E., 1955. "Separation of a supersonic turbulent boundary layer". *Journal of The Aeronautical Science*, Vol. 22, pp. 414–430.

Borgnakke, C. and Larsen, P. S., 1975. "Statistical collision model for Monte Carlo simulation of polyatomic gas mixture". *Journal of Computational Physics*, Vol. 18, pp. 405–420.

Camussi, R., Felli, M., Pereira, F., Aloisio, G., and DiMarco, A., 2008. "Statistical properties of wall pressure fluctuations over a forward-facing step". *Physics of Fluids*, Vol. 20, 075113.

Chapman, D. R., Kuehn, D. M., and Larson, H. K., 1958. "Investigation of separeted flows in supersonic and subsonic streams with emphasis on the effect of transition". NACA Report 1356.

Charwat, A. F., Roos, J. N., Dewey Jr., C. F., and Hitz, J. A., 1961a. "An investigation of separated flows – Part I: The pressure field". *Journal of Aerospace Sciences*,Vol. 28, pp. 457–470.

Charwat, A. F., Dewey Jr., C. F., Roos, J. N. and Hitz, J. A., 1961b. "An investigation of separated flows – Part II: Flow in the cavity and heat transfer". *Journal of Aerospace Sciences*, Vol. 28, pp. 513–527.

Charwat, A. F., 1971. "Separation of a supersonic accelerated flow over notches". *AIAA Journal*, Vol. 9, pp. 1656–1657.

Driftmyer, R. T., 1973. "A forward facing step study: the step height less than the boundary-layer thickness". NOLTR 73-98, Naval Ordinance Laboratory, White Oak, Maryland.

Everhart, J. L., 2009. "Supersonic/hypersonic laminar heating correlations for rectangular and impact-induced open and closed cavities". *Journal of Spacecraft and Rockets*, Vol. 46, pp. 545–560.

Garcia, A. L., and Wagner, W., 2000. "Time Step Truncation Error in Direct Simulation Monte Carlo". *Physics of Fluids*, Vol. 12, pp. 2621–2633.

Grotowsky, M. G., and Ballmann J., 2000. "Numerical investigation of hypersonic step-flows". *Shock Waves*, Vol. 10, pp. 57–72.

Hadjiconstantinou, N. G., 2000. "Analysis of Discretization in the Direct Simulation Monte Carlo". *Physics of Fluids*, Vol. 12, pp. 2634–2638.

Hinderks, M., Radespiel, R., and Gülhan, A., 2004. "Simulation of hypersonic gap flow with consideration of fluid structure interaction". In *34th AIAA Fluid Dynamics Conference and Exhibit*, AIAA Paper 2004–2238, Portland, OR.

Hinderks, M. and Radespiel, R., 2006. "Investigation of hypersonic gap flow of a reentry nosecap with consideration of fluid structure interaction". In *44th AIAA Aerospace Sciences Meeting and Exhibit*, AIAA Paper 2006-0188, Reno, NV, USA, January 9–12, 2006.

Howell, R. H., and Korst, H. H., 1971. "Separation controlled transonic drag-Rise modification for V-shaped notches". *AIAA Journal*, Vol. 9, pp. 2051–2057.

Leite, P. H. M., and Santos, W. F. N., 2009a. "Direct Simulation of Low Density Hypersonic Flow over a Foward-Facing Step". In *20th International Congress of Mechanical Engineering*, COBEM 2009, November 15–20, Gramado, RS, Brazil.

Leite, P. H. M., and Santos, W. F. N., 2009b. "Numerical Investigation of Heat Transfer and Pressure Distribution of Hypersonic Flow over a Forward-Facing Step". In *30th Iberian-Latin-American Congress on Computational Methods in Engineering*, CILAMCE 2009, November 5–8, Armação de Búzios, RJ, Brazil.

Leite, P. H. M, 2009. "Direct Simulation of the Step Influence on a Reentry Vehicle Surface (in Portuguese)". MS Dissertation, INPE.

Mazaheri, A. and Wood, W. A., 2009. "Heating augmentation for short hypersonic protuberances". *Journal of Spacecraft and Rockets*,Vol. 46, pp. 284–291.

Morgenstern Jr., A. and Chokani, N., 1994. "Hypersonic flow past open cavities". *AIAA Journal*, Vol. 32, pp. 2387–2393.

Nestler, D. E., Saydah, A. R., and Auxer, W. L., 1969. "Heat transfer to steps and cavities in hypersonic turbulent flow". *AIAA Journal*, Vol. 7, pp. 1368–1370.

Pan, F., and Acrivos, A., 1967. "Steady flows in rectangular cavities". *Journal of Fluid Mechanics*, Vol. 28, pp. 643–655.

Petley, D. H., Smith, D. M., Edwards, C. L. W., Carlson, A. B., and Hamilton II, H. H., 1984. "Surface step induced gap heating in the shuttle thermal protection system". *Journal of Spacecraft and Rockets*, Vol. 11, pp. 156–161.

Pullin, D. I., and Harvey, J. K., 1977. "Direct simulation calculations of the rarefied flow past a forward-facing step". *AIAA Journal*, Vol. 15, pp. 124–126.

Rogers, E. W. E., and Berry, C. J., 1965. "Research at the NPL on the influence at supersonic speeds and low Reynolds

numbers of thick laminar boundary layers". *Advances in Applied Mechanics: Rarefied Gas Dynamics* (ed. J. H. Leeuw, J. H.), Vol. I, Suppl. 3, pp. 574–591, Academic Press, New York.

Stüer, H., Gyr, A., and Kinzelbach, W., 1999. "Laminar separation on a forward facing step". *Eur. J. Mech. B/Fluids*, Vol. 18, pp. 675–6920.

Wilkinson, P. R. and East, R. A., 1968. "Mean properties of a region of separation in laminar hypersonic flow". *AIAA Journal*, Vol. 6, pp. 2183–2184.

Uebelhack, H. T., 1969. "Turbulent flow separation ahead of forward facing steps in supersonic two-dimensional and axisymmetric flows". Report VKI-TN-54, Von Karman Institute for Fluid Dynamics.

Vharbonnier, J., and Boerrigter, H., 1993. "Contribution to the study of gap induced boundary layer transition in hypersonic flow". In *AIAA/DGLR 5th International Aerospace Planes and Hypersonics Technologies Conference*, AIAA Paper 93–5111, Munich, Germany.

Zukoski, E. E., 1967. "Turbulent boundary-layer separation in front of a forward-facing step". *AIAA Journal*, Vol. 5, pp. 1746–1753

8. RESPONSIBILITY NOTICE

The authors are the only responsible for the printed material included in this paper.